Field characterization of an air-coupled micromachined ultrasonic capacitance transducer

A. G. Bashford
Department of Engineering, University of Warwick, Coventry CV4 7AL, England

David W. Schindel[a)]
Department of Physics, Queen's University, Kingston, Ontario K7L 3N6, Canada

David A. Hutchins and W. M. D. Wright
Department of Engineering, University of Warwick, Coventry CV4 7AL, England

(Received 21 September 1995; accepted for publication 24 August 1996)

Investigations into the field characteristics of an air-coupled ultrasonic capacitance transducer have been performed for a range of transducer configurations. The field of a 2-MHz bandwidth silicon backplate capacitance transducer has been scanned in air using a 1-mm-diam miniature detector at frequencies of up to 1.5 MHz. The radiated peak sound-pressure field is compared to theory based on a plane piston approach for various driving signals, namely pulsed and tone burst excitation. Aperture modifications, such as an annulus and a zone plate, have also been investigated and the devices have been shown to behave as predicted by theory. © *1997 Acoustical Society of America.* [S0001-4966(97)06012-8]

PACS numbers: 43.38.Bs, 43.58.Vb [SLE]

INTRODUCTION

The transduction of ultrasonic signals in air has gained increased interest recently, due to applications such as noncontact imaging for materials evaluation, distance ranging, and robotics. Such applications require a wide range of ultrasonic frequencies in air, and for materials evaluation, in particular, it is of distinct advantage to operate in the MHz range, where wavelengths in air become less than 1 mm. There are several designs of the ultrasonic transducer that can be used in air, but those useful at high frequencies tend to be based on either piezoelectric or capacitance (electrostatic) effects.

The major problem with conventional piezoelectric ceramic elements (such as PZT) is the large impedance mismatch at the boundary between the piezoelectric element and the surrounding air boundary. The efficiency of these devices for coupling into air can be increased by several methods, such as using a metal diaphragm[1] to act as a vibrating membrane, or by attaching a quarter wavelength impedance matching the layer to the front face. These impedance matching layers need to have a much lower acoustic impedance than the piezoelectric element, and only a small selection of materials can be used, such as silicon rubber,[2] epoxy resin-quartz,[3] and aerogels.[4] Further developments have reduced the impedance mismatch with the use of a 1–3 connectivity piezocomposite active element containing piezoceramic pillars in a polymer matrix.[5] The performance can be optimized for any particular application by changing the piezoceramic pillar fraction, shape, and distribution. In general, however, it is found that such devices are optimized for narrow bandwidth operation, and recent applications have used them in such a mode.[6] Other work has been reported in thick aerospace structures.[7]

The alternative method, which is investigated here, is to use a capacitance design, where a thin membrane is attached to a contoured, conducting rigid backplate. Such devices have been studied extensively in past work, which has investigated their response in relation to the backplate topography for metal backplates. The surface of a backplate for a capacitance transducer can either be textured (as in a roughened surface) or machined (as in a V-groove backplate). A variety of techniques for producing textured backplates have been investigated, including chemical etching, mechanical machining, and shot peening.[8] Some recent research has produced backplates by either depositing polyamide ridges,[9] machining, or etching to form regular patterns such as grooves and holes on or into a polished backplate. The results shown by Refs. 10 and 11 for V-grooved transducers suggest that the resonance frequency can quantitatively be predicted from the dimensions of a V-groove with a 90% confidence limit. It was also shown that a lumped parameter approximation could be used to describe the transducer by an equivalent electrical circuit. Both the resonance frequency and sensitivity could accurately be predicted.

Although such devices are useful, a more extended frequency response is available from new designs of transducer, based on silicon micromachining technology.[12] Various configurations have been described, including devices machined with an *in situ* front membrane.[13] The design to be studied here uses a silicon backplate into which miniature cylindrical pits have been etched chemically, leading to a typical construction as shown in Fig. 1.[14] The details of how such devices are constructed and characterized have been given elsewhere,[14] and some applications described.[15–18] Briefly, the backplate contains a series of uniformly spaced holes,

[a)]Corresponding author. Present address: Institute for Aerospace Research, National Research Council, Montreal Road, Building M-14, Ottawa, Ontario K1A 0R6, Canada. Fax +1-613-952-7136; Electronic mail: david.schindel@nrc.ca

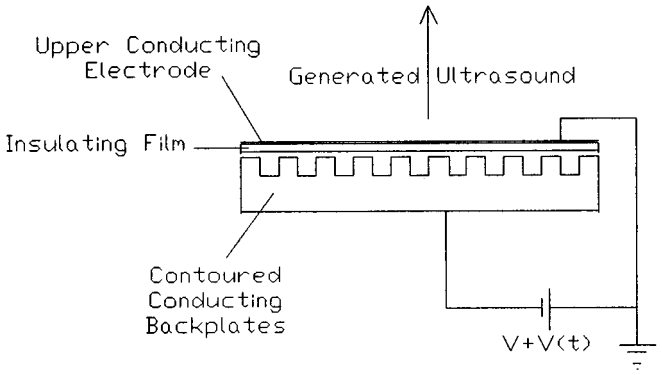

FIG. 1. Schematic diagram of a silicon backplate air-coupled transducer.

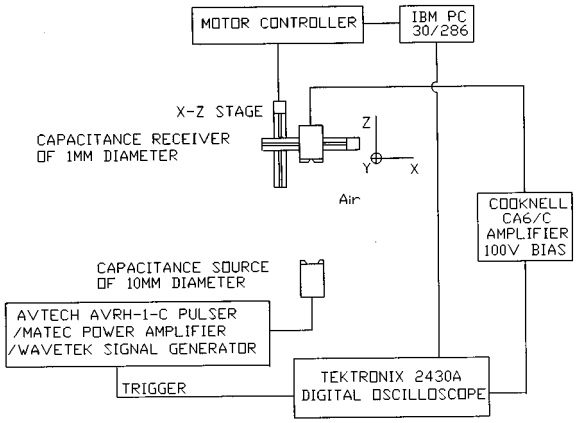

FIG. 2. Schematic diagram of the scanning system used.

etched into the top surface of a flat rigid silicon wafer. Gold is then evaporated onto the etched surface to produce a conducting backplate. A 5-μm Kapton polymer membrane (with a conducting top surface) is placed on top of the etched silicon backplate for both the source and receiver, trapping pockets of air. Applying a transient voltage between the backplate and the grounded front metallized surface of the membrane forces the membrane into motion, thus generating ultrasound in air. Detection can be achieved using an identical device, but a dc polarization voltage is required so that dynamic charges are induced on the backplate by motion of the membrane. Advantages of the above devices include the ease of manufacture, and the ability to reproduce field characteristics by introducing controlled surface roughness. Using the construction of the backplate outlined above, the transducer was found to have a good response into the MHz region, well-damped and with excellent sensitivity. As will be shown, with additional modifications to the aperture it is possible to produce transducers with increased axial intensities, thus making these devices ideal for a range of imaging applications.

As micromachined devices can be constructed with reproducible responses,[14] it is possible to study the radiated fields and waveforms for different drive waveforms and external apertures. The aim of the present paper is thus to compare the peak sound-pressure field of a micromachined silicon backplate capacitance transducer to that predicted by theory for a plane piston, and to extend this to transducer configurations (an annulus and a zone plate) which increase axial responses in air, for different voltage drive signals.

I. APPARATUS AND EXPERIMENT

The pressure waveforms throughout the field of micromachined capacitance transducers were measured in air using a scanned miniature hydrophone. The source transducers under test were derived from a device with a polished flat silicon backplate containing 40-μm-diam etched cylindrical pits of 40-μm depth[14] fitted with a 5-μm Kapton polymer membrane, and which had a 10-mm-diam active area. They were fitted with a grounded brass case, as described in Ref. 14, where additional detail of construction can be found. The scanned receiver was made in the same way, but was fitted with a 1-mm-diam aperture to define a limited detection area. Although bandwidths in excess of 2 MHz were available for both source and receiver, source driving frequencies were restricted to an upper limit of 700 kHz, where the wavelength in air is approximately 0.47 mm. Hence, at the upper frequency limit, the detector is approximately two wavelengths in diameter. In the experiment illustrated in Fig. 2, the apertured receiver was scanned over a two-dimensional horizontal plane throughout the field of the radiating transducer (the x-z plane), with the source radiating horizontally along the z axis. Scanning was achieved using a computer-controlled system which consisted of an IBM model 30 286 PC, controlling a Tektronix 2430A digital oscilloscope and a Modulynx motor controller, the latter driving two DAEDAL linear stages (one for each axis). Each stage was fitted with a synchronous stepping motor having 400 steps per revolution giving an absolute resolution of 0.005 mm and a positional accuracy of ± 0.004 mm/50 mm of travel for the system. The scans were performed with a 0.5-mm spatial resolution in the x (radial) direction and a 1-mm resolution in the z (axial) direction. A typical x-z scan area was 20 mm in the x direction and 50 mm in the z direction, with the field starting at 15 mm from the front face of the transducer membrane. All the scans were performed at atmospheric pressure, room temperature (20 °C) and low relative humidity (30%).

The source was excited with both wide bandwidth transients and tone bursts. A Matec 5100 gated power amplifier and a Wavetek 191 signal generator was used to drive the source with 350-V tone bursts of approximately 20 cycles at various frequencies in the 300- to 700-kHz range, whereas an Avtec AVRH-1-C pulser unit was used to provide a transient pulsed excitation with a width adjustable from 0.1–10 μs. The signal produced by the 1-mm apertured receiver was sent to a Cooknell CA6/C charge sensitive amplifier with a gain of 250 mV/pC, which also supplied a 100-V bias between the backplate and the membrane of the receiver. The nominal capacitance of the device was 650 pF. The signal waveform at each field position was digitized using a Tektronix 2430A oscilloscope, and stored on the PC. The peak sound-pressure variations were obtained from stored wave-

forms by taking the maximum peak-to-peak amplitude of the signal at each designated point.

II. RESULTS AND COMPARISON TO THEORY

A. Fields of a plane piston

Field variations in front of a transducer can be predicted by considering the interference of two components: plane wave from the source, and an inverted wave from the edge (referred to as the ''edge'' wave). Edge waves are diffracted from the aperture or at the boundaries of the source, and travel toward the axis of the transducer, thus interfering with the plane wave.[19–21]

The peak pressure variations in air for any size of aperture can be predicted, using established theory for the radiated field of a plane piston transducer.[19–21] The mathematical model assumes that the pressure at any point across and away from the transducer face can be computed from the interference of the plane and edge components, and also assumes that the front face is vibrating with a uniform amplitude and phase (although variations in these parameters can be included if required). The relevant expression for the time-dependent velocity potential at any given observation point in a half-space can be derived, and further details can be found in the quoted publications. Briefly, the velocity potential impulse response $\Phi(M,t)$ of a plane piston can be written as a combination of plane and edge wave components:

$$\Phi(M,t)=c|A|\underset{\text{(Plane wave)}}{\mathbf{H}(t-t_0)}+(c/2\pi)\Omega(ct)\underset{\text{(Edge wave)}}{\mathbf{H}(t-t_1)\mathbf{H}(t_2-t)}, \tag{1}$$

where M is the observation point, c is the longitudinal wave velocity, t is time, t_1 and t_2 are as defined below, and $\mathbf{H}$ is the Heaviside step function. The value of $|A|$ in the plane-wave component depends on the field position. For M opposite the front face the value is 1. For a field position such that $x=a$, the value drops to 1/2, and $|A|$ is zero at greater radial (x) distances, i.e., beyond the physical edge of the transducer. The time taken for an edge wave to reach the observation point from the closest and furthest edge of the piston is given by t_1 and t_2, respectively. In the case of a circular piston, $\Omega(ct)$ represents the angle of equidistant arc which is an analytical expression derived for the edge wave diffraction impulse response,[19–21] and is given by

$$\Omega(ct)=2\cos^{-1}\{[(ct)^2-z^2+x^2-a^2]/2x[(ct)^2-z^2]^{1/2}\}, \tag{2}$$

where a is the piston radius, x is the radial distance from the center, and z is the axial distance from the piston. The arrival times t_0 (for the plane wave), t_1 and t_2 are given by

$$t_0=z/c, \tag{3}$$

$$t_1=\{(a-x)^2+z^2\}/c, \tag{4}$$

$$t_2=\{(a+x)^2+z^2\}/c. \tag{5}$$

The pressure impulse response $\mathbf{S}(M,t)$ for an arbitrary point M is defined as the differential of the velocity potential impulse response, i.e.,

$$\mathbf{S}(M,t)=\rho_0(\delta\Phi/\delta t)(M,t), \tag{6}$$

where ρ_0 is the density of the medium. Equation (6) is only valid for values of t which are greater than or equal to t_0 and less than or equal to t_2; elsewhere $\mathbf{S}(M,t)=0$. The actual pressure waveform $\mathbf{P}(M,t)$ is then obtained by convolving the simulated motion of the piston [i.e., the velocity waveform $\nu(t)$] with the pressure impulse response for each spatial point:

$$\mathbf{P}(M,t)=\nu(t)\cdot\mathbf{S}(M,t), \tag{7}$$

where $\mathbf{P}(M,t)$ is the pressure response.

An additional factor is attenuation, which causes amplitude degradation and phase shifting. This can be high in air at ultrasonic frequencies, and so this factor needs to be incorporated into the model. The effect can be predicted using previous studies[22,23] and recent work has produced an experimentally derived expression[24] used here, which is

$$\sigma=15.895\times10^{-11}(T/T_0)^{1/2}f^2/(P/P_0), \tag{8}$$

where σ is the peak sound-pressure attenuation per meter (dB/m). The numerical constant in Eq. (8) is an experimentally measured value, determined at a constant temperature of 25 °C (Ref. 24) and f is the frequency (Hz). Here, T is the measured temperature, T_0 is the reference temperature, P is the measured pressure, and P_0 is the reference pressure. In the present work, T and P are taken as the standard reference values (25 °C and 101.325 kpa, respectively), and thus both T/T_0 and P/P_0 are unity. The attenuation was calculated at each field position by taking the Fourier transform of the predicted waveform, to give a frequency spectrum of the signal. This was then modified according to the expression for the calculated attenuation σ, so that the higher frequencies were suppressed more than the lower frequencies. An inverse Fourier transform then gave the resultant attenuated waveform. The resultant spatial variations were found as before by taking the peak-to-peak amplitude of the signal. Note that low humidity levels (30%) were maintained throughout the experiments; while water vapour is known to affect attenuation, its effect is small at high frequencies.[25]

To obtain the required theoretical velocity waveform of the vibrating membrane of the capacitance transducer [$\nu(t)$ in Eq. (7)] it was assumed that a small dc polarized component is always present on the membrane; thus we can assume the devices have a linear response[26] (i.e., the force is proportional to the drive voltage and hence the displacement). The Avtec pulser was used to provide a square wave with a 0.15-μs rise time and a width of 0.7 μs as the driving signal. This was filtered between 100 and 800 kHz (typical bandwidth for a source with a small dc bias), and the velocity waveform hence obtained by the differential with respect to time of the drive waveform. The predicted velocity waveform is shown in Fig. 3(a), and was used as $\nu(t)$ in the above theoretical predictions. The predicted theoretical sound-pressure waveform at an axial distance of 15 mm is shown in Fig. 3(b). This may be compared to the experimental waveform of Fig. 3(c), detected by the miniature scanned detector at the same position, where reasonable agreement with theory is evident.

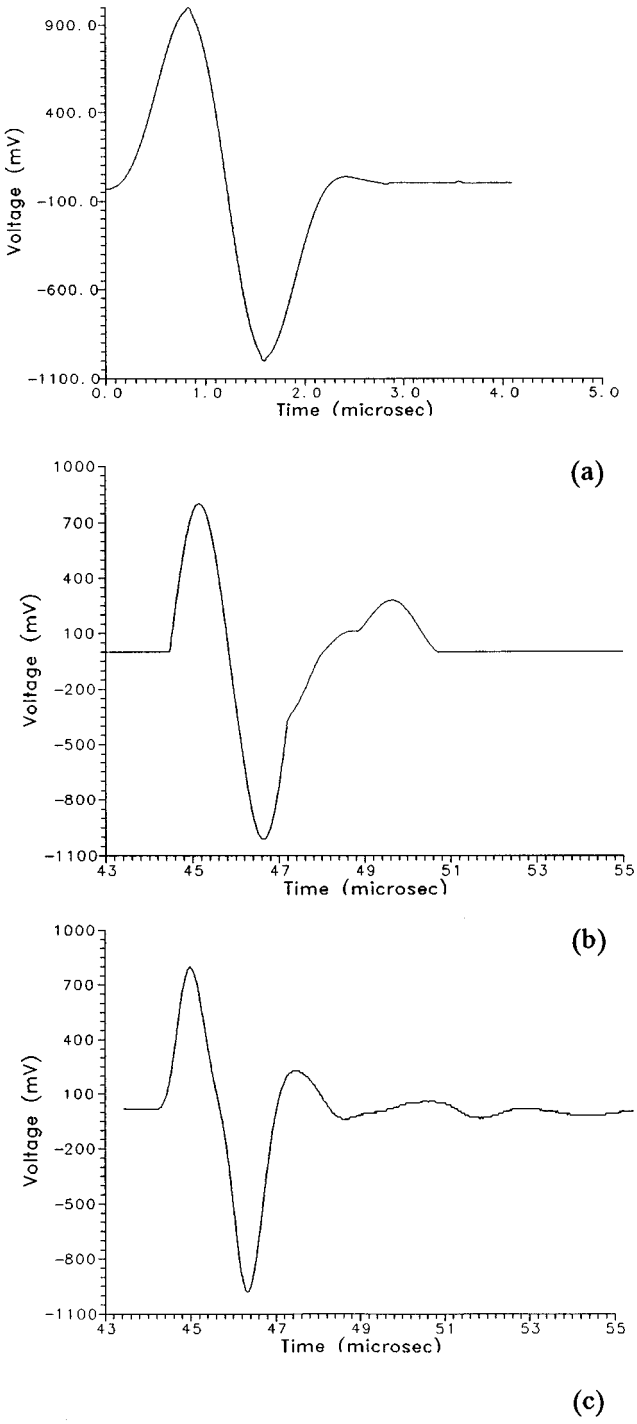

FIG. 3. (a) Predicted velocity waveform of the membrane. (b) Theoretical axial pressure waveform at $z=15$ mm, and (c) corresponding experimental waveform.

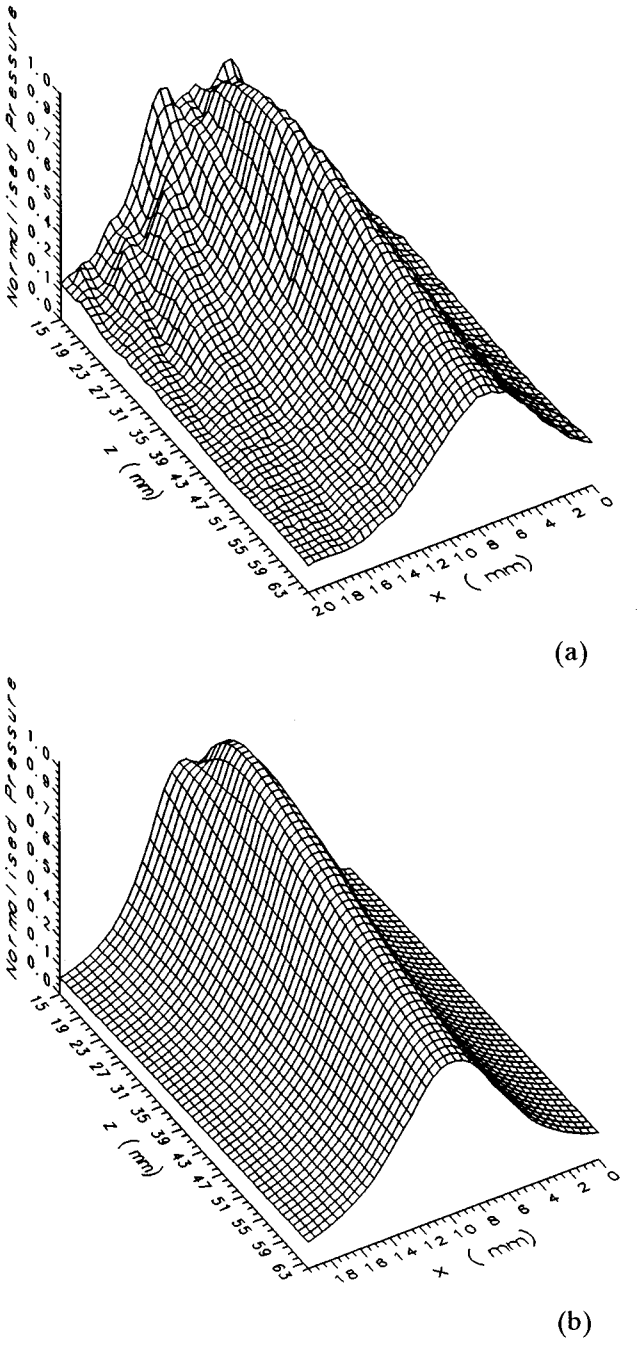

FIG. 4. (a) Experimental peak sound pressure variations, (b) theoretical peak sound-pressure variations, for a plane piston driven by a pulse centered at 316 kHz.

Peak sound-pressure spatial variations were now measured for a 10-mm-diam plane piston, using a 350-V drive pulse from the Avtec pulser unit. The driving pulse width was varied to give a plane-wave pressure component close to the transducer face in the form of a bipolar square wave pulse of variable width, and hence with a predetermined center frequency. The experimental and theoretical variations in peak sound-pressure waveform amplitude throughout the whole scanned field are presented in Fig. 4(a) for a drive excitation centred at 318 kHz. Remembering that this started 15 mm from the front face of the vibrating membrane, the remnants of the edge wave component can be seen clearly at the top left [i.e., at small axial (z) values], converging onto the axis to form the axial maximum by interference with the plane-wave component.

The predicted theoretical peak sound-pressure variations in air for a plane piston were now calculated using Eqs. (1)–(8), to compare to the experiment, the results being shown in Fig. 4(b) for the same scan area of 40 mm×20 mm. Good agreement is evident, with the near-field/far-field boundary positioned at the axial distance of approximately

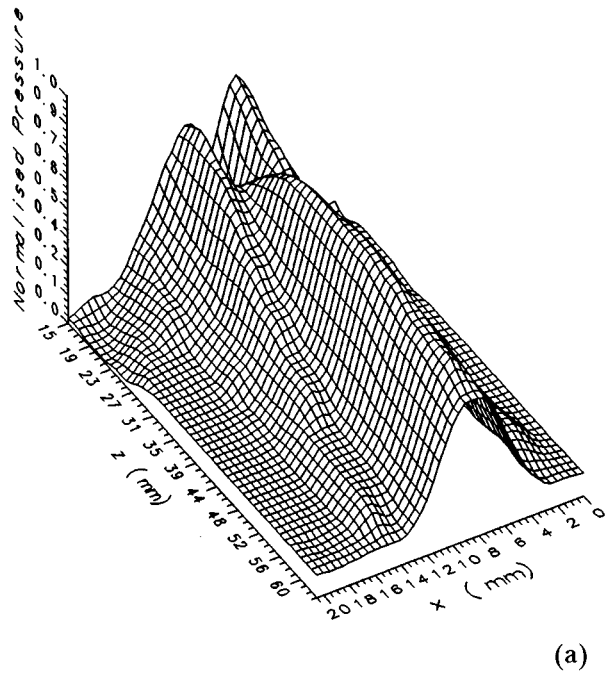

(a)

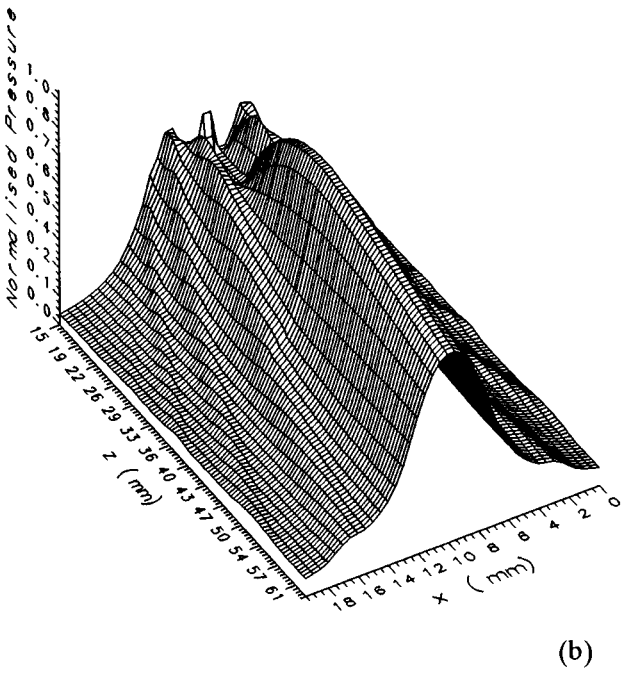

(b)

FIG. 5. (a) Experimental peak sound pressure variations, (b) theoretical peak sound-pressure variations, for a plane piston driven by a 500-kHz tone burst.

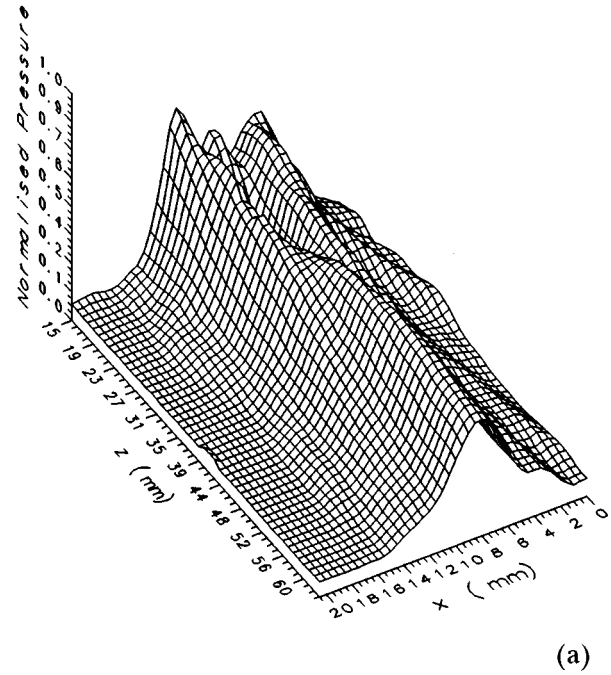

(a)

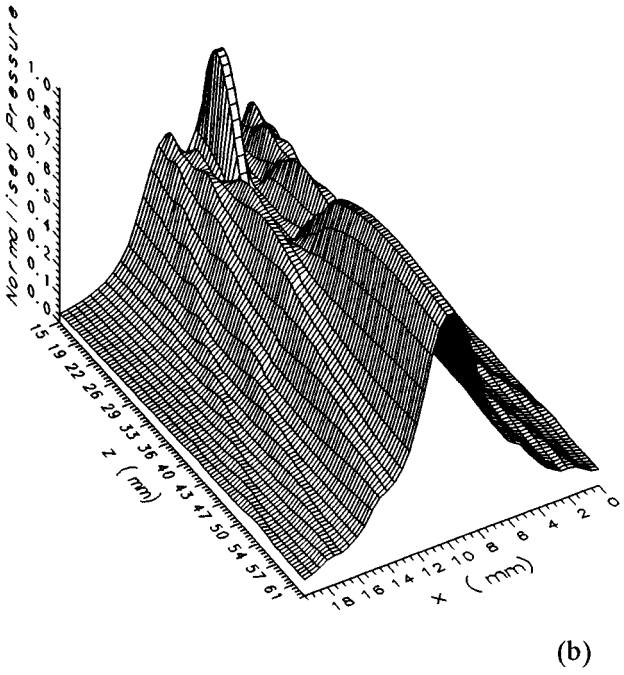

(b)

FIG. 6. (a) Experimental peak sound-pressure variations, (b) theoretical peak sound-pressure variations, for a plane piston driven by a 700-kHz tone burst.

24 mm, as expected from the quoted center frequency.

The above field plotting experiments were now repeated for tone burst excitation, using the Matec gated power amplifier to drive the transducers with a tone voltage signal containing 20 cycles. Figures 5(a) and 6(a) show the resulting spatial variations in peak sound-pressure amplitude in air, for excitation frequencies of 500 and 700 kHz, respectively. The corresponding theoretical plots for a plane piston, again including the correction for attenuation, are also presented in Figs. 5(b) and 6(b). For tone burst generation, the fields are more complicated theoretically, with marked theoretical axial variations in near-field amplitude, and the edge waves converging onto the axis. While some variations are present experimentally, these are not so evident. This is due to the finite aperture used in the receiver. Note, however, that the general features of near-field complexity and increased sidelobe levels are present, as expected for an excitation with a finite number of cycles (i.e., a narrower frequency bandwidth).

For completeness, an additional plot at 1.5 MHz is

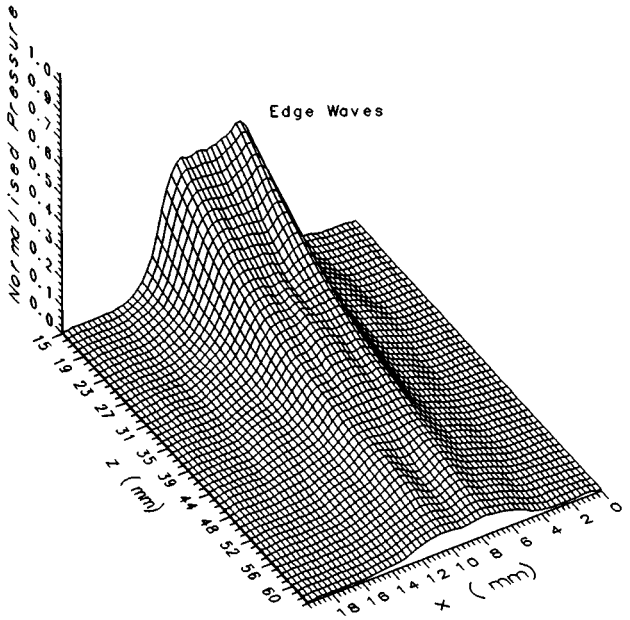

FIG. 7. Experimental peak sound-pressure variations for a plane piston driven by a 1.5-MHz tone burst.

shown in Fig. 7. This has a much faster amplitude decay with distance, but still has the recognizable features of a converging edge wave, and near-field interference effects. This rapid amplitude decay is due to several factors, one being the increased attenuation in air. However, because of the fact that the radiated wavelength is approximately 0.22 mm, and we are using a detector aperture of 1 mm, the scanned hydrophone cannot be assumed to give a wholly representative pressure plot. This increased directivity could cause the field plot to decay artificially, although attenuation at this frequency is probably the major factor.

The well-behaved nature of the emitted beam can be illustrated further by scanning in a plane perpendicular to the beam axis (i.e., in the X-Y plane). This is done in the near-field region for pulsed excitation centered at 500 kHz, 7 mm axially from the source [Fig. 8(a)], and at a distance of 50 mm [Fig. 8(b)] in the far field. Note the relatively smooth response in both cases, with the expected beam spreading in the far field.

Comparison of the above experimental scans with theoretical predictions show good qualitative agreement. However, the miniature detector does not have an absolute calibration, and probably has some directivity effects of its own at high frequencies. In addition, only relative peak sound-pressure amplitudes were plotted, and hence a quantitative comparison was not attempted.

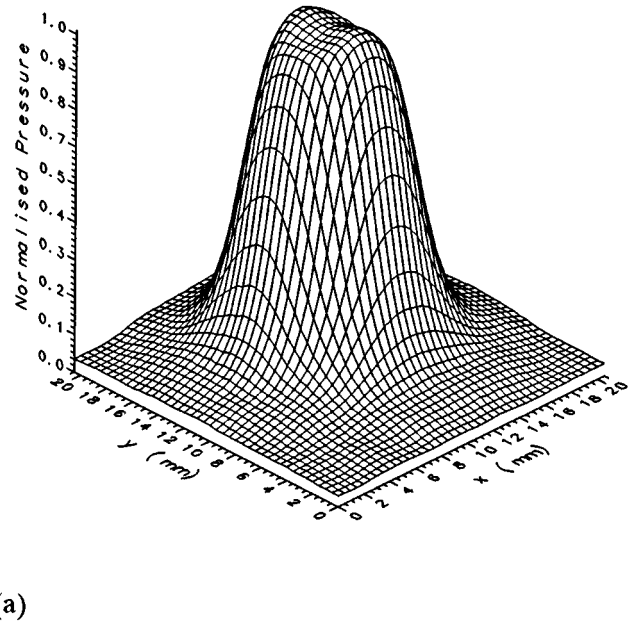

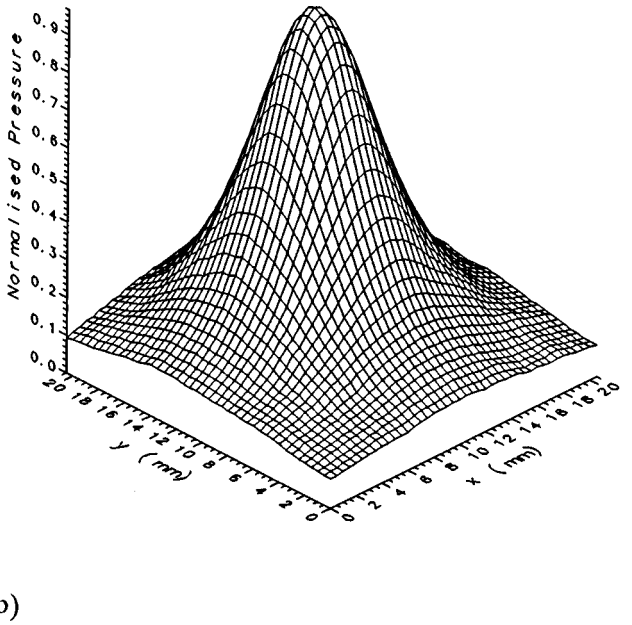

FIG. 8. Experimental peak sound-pressure variations in the X-Y plane for a plane piston transducer driven by a pulse centered at 500 kHz: (a) at 7 mm from the source; and (b) at 50 mm from the source.

B. Annular and zone plate transducers

An air-coupled annular transducer was produced by attaching a concentric 5-mm-diam paper disk to the center of the 10-mm-diam membrane. This absorbed radiated output over the 5-mm-diam central area, producing an annulus with an active inner diameter (d) of 5 mm and an outer diameter (D) of 10 mm. The peak sound-pressure field for this annulus was determined experimentally (as described above) for pulsed excitation with the Avtec pulser, giving a signal with a center frequency of 318 kHz. The results are shown in Fig. 9(a). Note the tendency for axial focusing, with a gradual increase in axial amplitude toward the maximum, accompanied by a smooth decrease in the direct radiation from the active area of the annulus. Similar features are seen in the theoretical plot, Fig. 9(b). This was produced by predicting the waveforms produced at each field point by two separate plane pistons, one of 10 mm diameter and the other of 5 mm

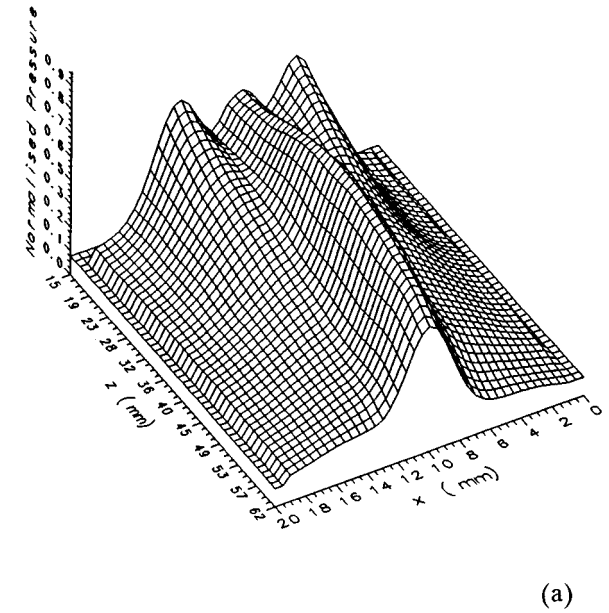

(a)

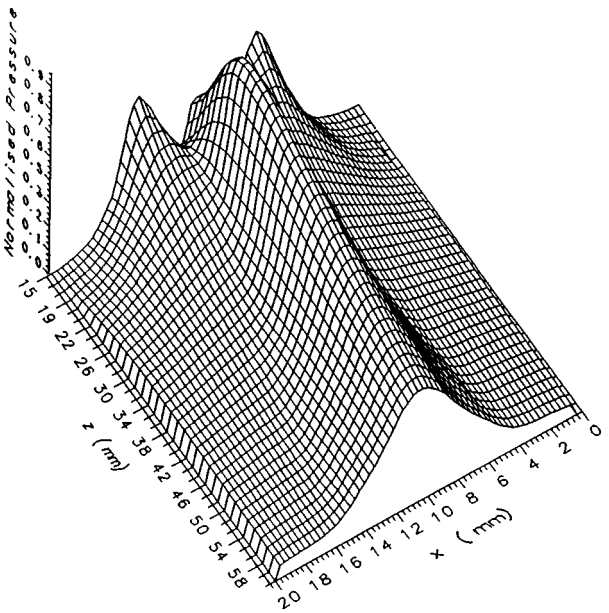

(b)

FIG. 9. (a) Experimental peak sound-pressure variations for an annulus, (b) theoretical pressure field plot for an annulus, using a pulse centered at 316 kHz ($d=5$ mm $D=10$ mm).

diameter. At each spatial point, the waveforms are then subtracted to predict the waveform of the annulus. Note that in the theoretical plot, the features are more sharp and less attenuated than those observed experimentally. This is again thought to be due, in part, to the finite receiver aperture. There also seems to be greater attenuation than that predicted by theory, a phenomenon that merits further investigation.

A zone plate consists of a series of active concentric rings (or zones), separated by areas that do not radiate. The zones are positioned such as to cause the radiated contributions from each zone to interfere constructively on-axis at the focal position, thus increasing the pressure intensity at the focus. The radial extent of each zone (R_M) is determined by

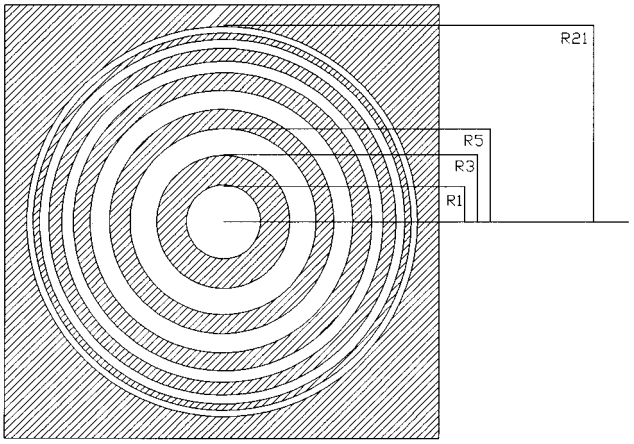

FIG. 10. Schematic diagram of a zone plate.

selecting the required axial focusing position Z_0 from the face of the zone plate (i.e., the focal length), and then positioning the edge of each zone to be at a distance $Z_0+M\lambda$ from position Z_0 where λ is the acoustic wavelength, and $M=1,3,5,7...$. As shown by Ref. 27, an approximate expression for the radial position of the edges of each zone (R_M) can be written as

$$R_m=\sqrt{\frac{M\lambda}{2}\left(Z_0+\frac{M\lambda}{8}\right)}. \tag{9}$$

Figure 10 shows a schematic diagram of a zone plate with six zones, with a predicted focal length from Eq. (9) of 7.5 mm when driven at a frequency of 500 kHz in air. The radii R_1, R_3, etc. are shown on the figure, with the unshaded areas representing regions where there is radiation; elsewhere, it is assumed that no emission occurs. In the present example, a central disk and five concentric annuli of emission were chosen, with the outer radius of the last zone (R_{21}) being 8 mm. This was thought to be a good compromise between focusing efficiency and ease of manufacture. The zone plate was etched chemically from sheet stainless steel of 0.13 mm thickness, using a computer-derived mask and photolithography. Concentric rings were held together by

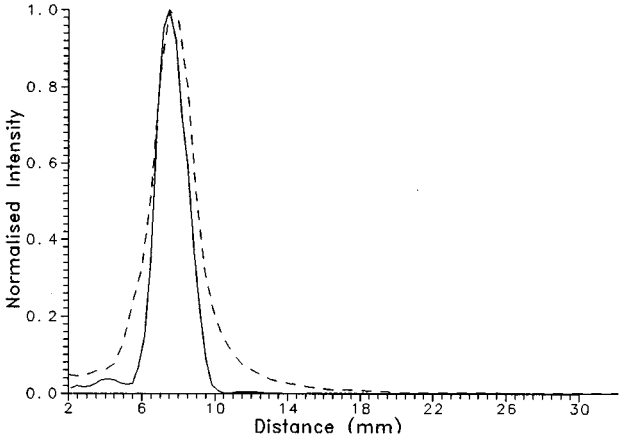

FIG. 11. Experimental (solid line) theoretical (dashed line) acoustic intensity axial plot, for a plane piston transducer with the zone plate.

thin radial bridges included in the original mask (not shown). This zone plate was placed across the transducer aperture, at a distance of 5 mm from the radiating membrane. Thus when a 500-kHz tone burst was applied to a transducer fitted with the zone plate, the axial pressure would be expected to increase to a maximum on axis at 7.5 mm from the plate (or 12.5 mm from the transducer face).

Figure 11 shows the experimental axial acoustic intensity field from the transducer, driven with a 500-kHz tone burst and fitted with the zone plate of Fig. 10. Note that now 2-D intensity variations (the square of the pressure amplitude) along the axis were plotted, to illustrate more graphically the focusing properties of these devices; due to the high noise floor on the experimental plot, pressure field variations off-axis did not correspond well to the theoretical result (this needs to be further investigated). It is evident, however that the transducer assembly has focused in air at the expected distance of 7.5 mm from the zone plate. Note the sharp focus, and the rapid axial decay of pressure amplitude at larger axial distances. Theoretically, the response of the zone plate can be simulated using the response of annuli as above. Here, the zone plate can be considered as a set of concentric annuli surrounding a central radiating disk; hence, the response can be found by adding the separate contributions of the central disk and each annulus in turn, for each field point. When this is done, the pressure field expected theoretically for 500-kHz tone burst generation in air is also shown in Fig. 11. In agreement with the predictions of Eq. (9), and the experimental observations of Fig. 11, the pressure amplitude peaks at 7.5 mm, and exhibits a rapid decay in amplitude at greater axial distances.

III. CONCLUSIONS

The experimental spatial variations in peak sound-pressure from an air-coupled micromachined capacitance transducer have been demonstrated to show many of the characteristics of a plane piston radiator. This was seen to be the case for both transient and tone burst voltage excitation. The theoretical model was modified to include frequency-dependent attenuation, and this was seen to improve agreement between theory and experiment. With additional modifications to the plane piston model, it was possible to predict the output from both annular and zone plate transducers, and this was again compared to experiment with reasonable agreement, indicating that axial pressures could be increased by both methods.

ACKNOWLEDGMENT

This work was funded by the Engineering and Physical Sciences Research Council (EPSRC).

[1] M. Babic, ''A 200-kHz Ultrasonic transducer coupled to the air with a radiating membrane,'' IEEE Trans. Ultrason. Ferroelectr. Freq. Control **UFFC-38**(3), 252–255 (1990).
[2] J. D. Fox and B. T. Khuri-Yakub, ''High frequency wave measurements in air,'' Proc. IEEE Ultrason. Symp. 581–592 (1983).
[3] P. Kleinschmidt and V. Magori, ''Ultrasonic remote sensors for non-contact object direction,'' Siemens Forsch. Entwicklungsber. **10** (2), (1981).
[4] O. Krauβ, R. Gerlach, and J. Fricke, ''Experimental and theoretical investigations of SiO_2-aerogel matched piezo-transducers,'' Ultrasonics **32**(3), 217–222 (1994).
[5] D. Reilly and G. Hayward, ''Through air transmission for ultrasonic non-destructive testing,'' Proc. 1991 IEEE Ultrason. Symp. 763–766 (1991).
[6] R. Farlow and G. Hayward, ''Real-time ultrasonic techniques suitable for implementing non-contact NDT systems employing piezoceramic composite transducers,'' Insight **36**, 926–935 (1994).
[7] C. M. Fortunko, J. O. Strycek, and W. A. Grandia, ''Nondestructive testing of ''thick'' aerospace honeycomb structures using through-transmitted ultrasonic guided waves,'' Rev. Prog. Quant. NDE **8B**, 1643–1650 (1990).
[8] W. S. H. Munro and C. Wykes ''Arrays for air-borne 100kHz ultrasound,'' Ultrasonics **32**(1), 57–63 (1994).
[9] M. J. Anderson, J. A. Hill, C. M. Fortunko, N. S. Dogan, and R. D. Moore ''Broadband electrostatic transducers; modelling and experiments,'' J. Acoust. Soc. Am. **97,** 262–272 (1995).
[10] H. Carr and C. Wykes, ''Diagnostic Measurements in capacitance transducers,'' Ultrasonics **31,** 13–20 (1993).
[11] M. Rafiq and C. Wykes, ''The performance of capacitive ultrasonic transducers using v-grooved backplates,'' Meas. Sci. Technol. **2,** 168–174 (1991).
[12] K. Suzuki, K. Higuchi, and H. Tanigawa, ''A silicon electrostatic ultrasonic transducer,'' IEEE Trans. Ultrason. Ferroelectr. Freq. Control **36,** 620–627 (1989).
[13] M. I. Haller and B. T. Khuri-Yakub, ''A surface micromachined electrostatic ultrasonic air transducer,'' Proc. 1994 Ultrason. Symp. 1241–1243 (1994).
[14] D. W. Schindel, D. A. Hutchins, L. Zou, and M. Sayer, ''The design and characterization of micromachined air-coupled capacitance transducers,'' IEEE Trans. Ultrason. Ferroelectr. Freq. Control **42,** 42–50 (1995).
[15] D. W. Schindel and D. A. Hutchins, ''Applications of micromachined capacitance transducers in air-coupled ultrasonics and nondestructive evaluation,'' IEEE Trans. Ultrason. Ferroelectr. Freq. Control **42,** 51–58 (1995).
[16] D. W. Schindel and D. A. Hutchins, ''Through-thickness characterization of solids by wideband air-coupled ultrasound,'' Ultrasonics **31,** 11–17 (1995).
[17] D. A. Hutchins, W. M. D. Wright, and D. W. Schindel, ''Ultrasonic measurements in polymeric materials using air-coupled transducers,'' J. Acoust. Soc. Am. **96,** 1634–1642 (1994).
[18] B. Hosten, D. A. Hutchins, and D. W. Schindel, ''Measurement of elastic constants in composite materials using air-coupled ultrasonic bulk waves,'' J. Acoust. Soc. Am. **99,** 2116–2123 (1996).
[19] P. R. Stepanishen, ''Transient Radiation from Pistons in an Infinite Planar Baffle,'' J. Acoust. Soc. Am. **49,** 1630–1638 (1971).
[20] J. C. Lockwood and J. D. Willette, ''High-Speed methods for computing the exact solution for the pressure variations in the nearfield of a baffled piston,'' J. Acoust. Soc. Am. **53,** 735–741 (1973).
[21] D. A. Hutchins and G. Hayward, ''The radiated field of ultrasonic transducers,'' in *Physical Acoustics, Vol. XIX*, edited by R. N. Thurston and A. D. Pierce (Academic New York, 1990), pp. 2–134.
[22] R. Hickling and S. P. Marin, ''The use of ultrasonics for gauging and proximity sensing in air,'' J. Acoust. Soc. Am. **79,** 1151–1159 (1986).
[23] H. E. Bass, L. C. Sutherland, and L. Evans, ''Atmospheric absorption of sound: Theoretical predictions,'' J. Acoust. Soc. Am. **51,** 1565–1572 (1972).
[24] L. J. Bond, C. Chiang, and C. M. Fortunko ''Absorption of ultrasonic waves in air at high frequencies (10–20 MHz),'' J. Acoust. Soc. Am. **92,** 2006–2015 (1992).
[25] H. E. Bass, L. C. Sutherland, and A. J. Zuckerwar, ''Atmospheric absorption of sound: Update,'' J. Acoust. Soc. Am. **88,** 2019–2020 (1990).
[26] D. W. Schindel and D. A. Hutchins, ''The capacitance transducer as a standard ultrasonic source in solids,'' J. Acoust. Soc. Am. **97,** 1650–1659 (1995).
[27] M. Z. Sleva, W. D. Hunt, and R. D. Briggs, ''Focusing performance of epoxy and air-backed polyvinylidene fluoride Fresnel zone plates,'' J. Acoust. Soc. Am. **96,** 1627–1633 (1994).